Published in final edited form as:
Org Biomol Chem. 2010 December 7; 8(23): 5431–5441. doi:10.1039/c0ob00482k.

Electronic structural dependence of the photophysical properties of fluorescent heteroditopic ligands – implications in designing molecular fluorescent indicators†

Ali H. Younes[a], **Lu Zhang**[a], **Ronald J. Clark**[a], **Michael W. Davidson**[b], and **Lei Zhu**[a]

Lu Zhang: lzhu@chem.fsu.edu; Michael W. Davidson: davidson@magnet.fsu.edu

[a]Department of Chemistry and Biochemistry, Florida State University, Tallahassee, FL 32306-4390, USA. Fax: +1 850 644 8281; Tel: +1 850 645 6813

[b]National High Magnetic Field Laboratory and Department of Biological Science, Florida State University, 1800 East Paul Dirac Drive, Tallahassee, FL 32310, USA. Fax: +1 850 644 8920; Tel: +1 850 644 0542

Abstract

Two fluorescent heteroditopic ligands (**2a** and **2b**) for zinc ion were synthesized and studied. The efficiencies of two photophysical processes, intramolecular charge transfer (ICT) and photoinduced electron transfer (PET), determine the magnitudes of emission bathochromic shift and enhancement, respectively, when a heteroditopic ligand forms mono- or dizinc complexes. The electron-rich **2b** is characterized by a high degree of ICT in the excited state with little propensity for PET, which is manifested in a large bathochromic shift of emission upon Zn^{2+} coordination without enhancement in fluorescence quantum yield. The electron-poor **2a** displays the opposite photophysical consequence where Zn^{2+} binding results in greatly enhanced emission without significant spectral shift. The electronic structural effects on the relative efficiencies of ICT and PET in **2a** and **2b** as well as the impact of Zn^{2+}-coordination are probed using experimental and computational approaches. This study reveals that the delicate balance between various photophysical pathways (*e.g.* ICT and PET) engineered in a heteroditopic ligand is sensitively dependent on the electronic structure of the ligand, *i.e.* whether the fluorophore is electron-rich or poor, whether it possesses a donor–acceptor type of structure, and where the metal binding occurs.

Introduction

The operation of a fluorescent indicator is based on sensitive and selective modulation of emission by an analyte species. The successful structural design of a fluorescent indicator relies on a thorough understanding of the analyte-sensitive photophysical processes.[1,2] Analyte-modulated photoinduced electron transfer (PET), intramolecular charge transfer (ICT), excited state proton transfer (ESPT), excimer/exciplex formation, fluorescence resonance energy transfer (FRET), and other processes have been employed in engineering fluorescent indicators.[3] So much experience has been accumulated in this area that a modular strategy in structural design by coupling a molecular recognition event with the efficiency of a single photophysical process has become routine.[4,5]

†Electronic supplementary information (ESI) available: Additional experimental procedures; cyclic voltammograms; Frontier molecular orbital diagrams, additional spectra and lifetime traces. CCDC reference number 786092. For ESI and crystallographic data in CIF or other electronic format see DOI: 10.1039/c0ob00482k

Correspondence to: Michael W. Davidson, davidson@magnet.fsu.edu; Lei Zhu.

In the course of our development of fluorescent indicators for zinc ion (Zn^{2+}) that are effective over large concentration ranges,[6] we have become interested in the fundamental aspects of fluorophores in which more than one photophysical processes are modulatable *via* molecular recognition.[7] One typical structure contains a fluorophore and two different Zn^{2+} binding sites, whose emission depends on the coordination status of the compound (see cartoon in Fig. 1 and compound **1** in the Structures). Much of our effort since the initial report of our "fluorescent heteroditopic ligands"[8] has been devoted to unraveling the finesse of the coordination-mediated photophysical processes in order to develop heteroditopic systems that afford large fluorescence contrast in their three coordination states (Fig. 1).[9,10] Three parameters are used for evaluating the 'fluorescence contrast': (1) the fluorescence enhancement upon monozinc complex formation (φ_1/φ_0), (2) emission band shift upon dizinc complex formation ($\Delta\lambda = \lambda_2 - \lambda_1$), and (3) the fluorescence quantum yields of both mono- and dizinc complexes (φ_1 and φ_2). The fluorescence quantum yield (φ) and emission wavelength (λ) values of compound **1** are listed in Fig. 1. We aim to increase the values for all three sets of parameters *via* structural modification, the success of which may lead to indicator molecules for Zn^{2+} with enhanced sensitivity across a large concentration range.

In our previous study on the monotopic arylvinyl-bipy-based fluorophores, an electron-rich aryl group was found to afford a large emission band shift upon Zn^{2+} complexation.[10] This finding potentially provides a solution to increase the value of the second parameter – *i.e.*, the emission band shift upon dizinc complex formation – in a heteroditopic ligand context. The cyclic voltammetric studies of the monotopic fluoroionophores led to a hypothesis, however, that the oxidation potential would increase when an electron-rich aryl group is incorporated, which is expected to impair the electron-accepting ability of the arylvinyl-bipy fluorophore in the excited state during a possible PET event in the heteroditopic framework (Fig. 1).[9] The attenuation of the PET efficiency may decrease the value of the first parameter – the fluorescence enhancement upon monozinc complex formation. In the current study, we have prepared two fluorescent heteroditopic ligands containing an electron-poor (**2a**) and an electron-rich (**2b**) aryl group, respectively. Their coordination-mediated photophysical properties were found to be consistent with our hypothesis.

Results and discussion

Structures

The structures of **1**, **2a**, **2b**, **3** and **4** are shown below.

Design

Heteroditopic compounds **2a** and **2b** were designed to have an electron-poorer and an electron-richer bipy-containing fluorophore, respectively, than that of the parent compound **1**. Compounds **3** and **4** are the respective monotopic bipy-containing fluorophores of **2a** and **2b**, devoid of the higher-affinity dipicolylamino (DPA) Zn^{2+}-binding site.[11] The electron-deficient nature of fluorophore **3** is expected to render the intramolecular PET process efficient in the excited state of the heteroditopic **2a**. However, the emission band shift of **2a** when the bipy site is coordinated is expected to be small because the fluorophore is expected to exhibit little charge transfer character in the excited state. Compound **2b** which contains an electron-rich fluorophore would instead have little thermodynamic driving force for intramolecular PET in the absence of Zn^{2+}. When Zn^{2+} binds at the bipy site, the emission bathochromic shift is expected to be significant due to the highly charge-transfer nature of fluorophore **4**.

The hypothesis on **2a** and **2b** is tested by various experimental and computational means which are described following the synthesis section. The characterization of the electronic

structures of **2a** and **2b** *via* cyclic voltammetry and DFT calculation will be presented first, followed by the description of their spectroscopic features. The acquired knowledge base will be used to explain the Zn^{2+}-binding-dependent emission of **2a** and **2b**. Finally, the potential of **2a** as an indicator for intracellular Zn^{2+} will be briefly evaluated.

Synthesis

The syntheses of the monotopic bipy-containing fluoroionophores **3** and **4** are presented in Scheme 1. Horner–Wadsworth–Emmons (HWE) reaction between phosphonate **5**[9] and 2-pyridinecarboxaldehyde produced the *trans* isomer of compound **3**. The synthesis of compound **4** was initiated by radical bromination of 2-methylthiophene **6** followed by an Arbuzov phosphonate synthesis to afford **8**. The HWE reaction between **8** and **9** resulted in **10** which was deprotected followed by a second HWE reaction with phosphonate **5** to afford compound **4**.

Dicarboxaldehyde **13b** was prepared by the Vilsmeier reaction[12] from **12** which was obtained by the HWE reaction between **8** and 2-thiophenecarboxaldehyde. The syntheses of **2a** and **2b** (Scheme 2) followed an established route.[13] Briefly, monoprotection of dicarboxaldehydes **13a** and **13b** afforded **14a** and **14b**, respectively. The subsequent reductive amination/deprotection sequence gave rise to **16a** and **16b**, which underwent the HWE reactions with phosphonate **5** to afford **2a** and **2b**, respectively.

X-Ray crystal structure of 2b

The single crystals of **2b** suitable for X-ray diffraction were acquired *via* slow evaporation of its solution in hexanes and CH_2Cl_2. Only one conformer with respect to the rotations of the single bonds in the fluorophore portion was observed. The dipoles of the four aromatic rings (two pyridyls and two thienyls) are alternating across the plane, presumably to minimize the overall dipole moment of the fluorophore. It is conceivable that in solution, the rotations of these single bonds may be permitted under ambient conditions to result in various conformers. Bipy units without conjugatable aromatic moieties attached usually display small dihedral angles (6–7° or slightly larger) along the C–C bonds.[8,14–16] The direct connection to a vinylaryl group such as in **2b**, tends to flatten the bipy unit to result in an extensively conjugated structure as shown in Fig. 2B. A similarly coplanar arylvinyl-substituted bipy was reported earlier.[10]

Computational studies and cyclic voltammetry

The charge-transfer characters, or the lack thereof, of compounds **3** and **4** are illustrated in their frontier molecular orbital diagrams (at B3LYP/6-31+G(d,p) level, Fig. 3). Little electron density redistribution is shown between the HOMO and LUMO of compound **3**. On the other hand, the electron density localizes on the divinylthienyl portion of compound **4** in its HOMO, which shifts to the bipy side in the LUMO. The difference in electron density distributions of the calculated frontier orbitals of **4** is consistent with an occurrence of charge transfer upon photoexcitation.

The HOMO diagrams (at B3LYP/6-31+G(d,p) level) of heteroditopic **2a** and **2b** are shown in Fig. 4. Compared to the monotopic precursor **3**, the HOMO of **2a** (Fig. 4A) localizes primarily on the tertiary amino group, which is part of the high-affinity DPA coordination site, instead of the electron-poor fluorophore on which HOMO-1 resides (Fig. S5). On the contrary, the HOMO of the electron-rich **2b** (Fig. 4B) occupies the divinylthienyl component of the fluorophore with a **π** character, similar to that of **4** (Fig. 3C).

The relative energies of frontier MOs can be used to gauge the relative efficiencies of PET in **2a** and **2b**.[9] The excitation of **2a** results in a $^1(\pi–\pi^*)$ state where an electron is elevated

from the HOMO-1 (which is a π orbital) to the LUMO (The HOMO to LUMO transition is of the forbidden n → π* nature,[17,18] evidenced by the low oscillator strength, 0.2, of this transition, see Table 2). As sketched in Fig. 4A, PET from the tertiary amino group-occupied HOMO (orbital diagrams of HOMO-1 and LUMO are shown in Fig. S5†), is thermodynamically favored, which leads to the nonradiative decay to the ground state. On the other hand in the excited **2b**, PET from the tertiary amino group, which is HOMO-3 (Fig. S6†), to the singly occupied HOMO is thermodynamically uphill (Fig. 4B). Therefore, fluorescence emission would occur instead accompanying the relaxation back to the ground state.

The energetic arrangement of HOMO and HOMO-1 or HOMO-3, which is critical in understanding the relative efficiencies of PET in heteroditopic ligands of the design shown in Fig. 1, is substantiated by cyclic voltammetric measurements. All ligands undergo irreversible electrochemical oxidation (Figures S1–S4†). The first anodic peak potential (E_{pa}) of **2b** (0.34 V in CH_3CN *vs.* Fc/Fc^+, Table 1) is attributed to the fluorophore moiety as it is close to the E_{pa} of the reference compound **4** (0.57 V); whereas the first E_{pa} of **2a** (0.65 V) is assigned to the tertiary amino group based on comparison with the published data involving dipicolylamino groups.[9,19] The E_{pa} of compound **3**, which is the fluorophore of **2a**, has a much higher value of 1.31 V.

Solvent effect on fluorescence

Normalized emission spectra of compounds **3** and **4** in various organic solvents are displayed in Fig. 5. Emission spectra of **3** have little dependence on solvent. On the other hand, compound **4** exhibits a greater positive solvatochromism.[20] The emission energy of **4** decreases rapidly as the polarity and/or the hydrogen bond donating ability of the solvent increases, consistent with emission from a highly polar, charge-transfer-type excited state.[21] The Stokes shifts of **3** and **4** in various solvents were plotted against the normalized Reichardt's $E_T(30)$ values (E_T^N) (Fig. 6).[22,23] In agreement with the observations by Tor, Castellano, and others,[24,25] the linearities of the two correlations, as determined by the correlation coefficients of the least-squares fits, are slightly better than those of the typical Lippert plots (Fig. S7†).[1] The slopes of the modified Lippert plots (Fig. 6) are proportional to the changes of molecular dipole upon photoexcitation ($\Delta\mu_{ge} = \mu_e - \mu_g$).[22] Therefore, a larger slope represents a greater degree of charge transfer in the excited state. Compound **4** which contains an electron-rich divinylthienyl group, undergoes a greater extent of charge transfer than compound **3**.

Fluorescence lifetime and quantum yield

A very low fluorescence quantum yield ($\varphi_f = 0.01$) was recorded for ligand **2a** in CH_3CN. Comparing to that of **3** (0.32) which is the fluorophore of **2a**, the incorporation of the DPA group reduces the fluorescence quantum yield by 32-fold, likely *via* a PET pathway as suggested in the computational analysis. Upon Zn^{2+} coordination at the saturation level to afford the dizinc complex, the quantum yield of **2a** is enhanced by 46-fold to 0.46. The fluorescence quantum yield of **2b** (also in CH_3CN), where no PET is expected based on the DFT calculations, is 0.20. Upon forming the dizinc complex, the φ_f, in contrast to **2a**, is reduced to 0.06. The model monotopic ligand **4** undergoes a similar reduction of quantum yield from 0.12 to 0.07 upon Zn^{2+} binding. The Zn^{2+}-coordination-mediated fluorescence quenching of arylvinylbipy fluorophores when the aryl group is highly electron-donating such as in **4** is consistent with our prior observation[10] where the reduction of radiative decay constant k_r, which is caused by Zn^{2+}-coordination enhanced excited state charge transfer outpaces the reduction of nonradiative decay constant k_{nr} when Zn^{2+} binds.

No lifetime was recorded for **2a** due to its very low fluorescence intensity. Coordination to Zn^{2+} greatly enhances the intensity, and results in a biexponential emission decay trace. The longer component (1.98 ns) is assigned to the emission from the Zn^{2+}-coordinated fluorophore because it is close in value to the lifetime recorded for the Zn^{2+} complex of the monotopic **3** (1.96 ns). **2b** shows monoexponential decay with a lifetime of 1 ns corresponding to emission from the fluorophore as compared to that of ligand **4** (τ = 0.98 ns). A biexponential decay is observed upon formation of the Zn^{2+}-complex of **2b**, where τ_1 (1.36 ns) is attributed to the Zn^{2+}-bound fluorophore. The longer τ_2 is currently unassigned; it may be related to an intramolecular exiplex species resulting from the interaction between the excited fluorophore and the Zn^{2+}-bound DPA group.[19]

Absorption and emission titration studies

Compound **2a** shows a major absorption band at 340 nm (blue in Fig. 7A), which is assigned to the HOMO-1 to LUMO (π–π^*) transition. As $ZnCl_2$ is added to the solution, the absorption maximum starts to decrease and transforms into a new band at 348 nm (red, Fig. 7A). On the other hand, **2b** shows absorption at a higher wavelength (418 nm, blue in Fig. 7B) which undergoes a larger bathochromic shift to 436 nm (red, Fig. 6B) upon coordination to $ZnCl_2$.

The emission spectra of **2a** and **2b** are shown in Fig. 8. **2a** shows a very weak emission under the irradiation from a handheld UV lamp (λ_{ex} = 365 nm, see the inset of Fig. 8A). However, as $ZnCl_2$ is added, an enhancement in fluorescence intensity was observed with a bright blue fluorescence being observed under the UV lamp excitation.

Provided with the knowledge base acquired from the experimental and computational investigations described in the previous sections, the Zn^{2+}-coordination dependent fluorescence of **2a** and **2b** can be explained. The weak fluorescence of **2a** results from an efficient nonradiative PET process from the dipicolylamino (DPA) moiety to the excited fluorophore. The fluorophore has an oxidation potential that is lower than that of the tertiary amino group in DPA, thus providing the thermodynamic driving force for PET. Such an electron transfer occurrence is also supported by computational studies where the HOMO of **2a** is mainly localized on the tertiary amino group and HOMO-1 is found as a π orbital extending over the plane of the fluorophore. Upon coordination to Zn^{2+}, the oxidation potential of the DPA group is expected to be lowered, thus reducing the thermodynamic driving force of the fluorescence-quenching PET to result in the enhancement of emission. Along an increasing Zn^{2+} gradient (Fig. 9), two factors may contribute to the enhancement of fluorescence intensity. One is the blocking of the PET process upon monozinc complex formation. The other is attributed to the coordination of Zn^{2+} to the bipy-containing fluorophore, which reduces the rotational freedom of the molecule, leading to an additional enhancement in fluorescence quantum yield.

Although a remarkable enhancement in emission is recorded, **2a** is not significantly bathochromically shifted upon dizinc complex formation (1000 cm^{-1}, Table 3). The observed behavior can be explained with assistance from the solvatochromic and computational studies of fluorophore **3**. Increasing polarity, especially the hydrogen bond donating ability of the solvent, which would specifically interact with the pyridyl nitrogens in **3**, does not lead to a significant bathochromic shift in the emission of **3** (Fig. 5). This observation leads to the conclusion that there is only a very modest degree of charge transfer, presumably from the vinylpyridyl to the bipy moiety, upon the excitation of **3**. This is supported by little electron density rearrangement between the HOMO and the LUMO of **3** (Fig. 3), when compared to those of fluorophore **4**. The placement of the cation Zn^{2+} at the bipy end of **2a** would not significantly affect the stability of a relatively nonpolar excited

state structure. Therefore, only a small degree of bathochromic shift was observed when the dizinc complex of **2a** was formed.

However, monotopic ligand **3** shows a larger emission bathochromic shift upon Zn^{2+} coordination than that of **2a** (Table 3, see also Fig. S12†). The difference can be explained by examining the coordination status of the lone pyridyl group in the fluorophores of **2a** and **3** (marked by a red 'X' in Fig. 9) over the titration processes. In **2a**, the lone pyridyl group is involved in the formation of the monozinc complex, thus leading to the reduction or elimination of the even modest charge-transfer capacity of the pyridylvinyl-bipy excited state. Therefore, the subsequent binding of Zn^{2+} at the bipy position alters little the energy of the excited state. In the monotopic compound **3**, however, the monozinc complex formation occurs at the bipy site with the lone pyridyl group unbound (Fig. 9). Charge transfer, albeit modest, still occurs from the pyridylvinyl group to the bipy site upon excitation which is stabilized by the presence of Zn^{2+} at the bipy site, leading to the observed bathochromic shift in emission (Fig. S12†).

Ligand **2b**, on the other hand, shows an initial minimally blue shifted Zn^{2+}-induced enhancement.[8] The emission of **2b** is subsequently decreased upon further Zn^{2+} addition with a significant red shift (3079 cm^{-1}, Table 3) where the emission color changing from green to orange (Fig. 8B, inset). The later rise of emission of **2b** centered at 600 nm is due to the coordination of Zn^{2+} at the bipy site. Opposite to the observations on **2a**, the fluorescence quantum yield of **2b** suffers reduction when complexed to Zn^{2+}. Such a behavior can be understood from the computational and cyclic voltammetric studies which show that there is no driving force for PET in the free ligand of **2b**. The absence of PET is reflected in the recorded monoexponential decay of **2b** with lifetime of 1.00 ns, corresponding to emission from the fluorophore. Without the PET pathway in the free ligand of **2b**, coordination of Zn^{2+} at DPA position would not enhance the fluorescence. Rather, there is the possibility of "oxidative photoinduced electron transfer" of the fluorophore, where the Zn^{2+}-bound DPA groups are the electron acceptors from the excited, electron-rich fluorophore.[26–28] When the dizinc complex of **2b** is formed, Zn^{2+}-coordination at the bipy site significantly enhances the charge-transfer character of the fluorophore, which leads to a lower rate of radiative decay. Both oxidative PET and coordination-enhanced charge-transfer at bipy may contribute to the reduction of the fluorescence quantum yield of **2b** when either mono- or dizinc complex is formed.

With the applications of heteroditopic ligands in detecting and quantifying free Zn^{2+} (unbound with protein molecules or other ligands) in biological systems in mind,[30–34] we investigated the Zn^{2+}-dependent fluorescence of **2a** under simulated physiological conditions.[6,19,35–37] The fluorescence spectra of **2a** were collected over an increasing Zn^{2+} gradient. The free Zn^{2+} concentrations ($[Zn]_f$) were controlled by a buffering system containing various metal chelators[38] and were estimated using "Webmaxc Standard", a program developed for analyzing buffered metal ion solutions.[29] The absorption spectrum of ligand **2a** was slightly red shifted (12 nm) at the completion of the titration experiment due to coordination to bipy of the fluorophore (Fig. S10†). Data in Fig. 10 depicts the emission behavior of **2a** in an aqueous buffer. A fluorescence quantum yield (φ_f) of 0.012 was recorded for the free ligand. Addition of Zn^{2+} results in a dramatic increase in emission. A φ_f of 0.57 was determined at the saturation level (the red spectrum in Fig. 10), presumably of the dizinc complex. The calibration curve of emission intensity at 400 nm *versus* $[Zn]_f$ shown in the inset reveals that the emission is most sensitive to $[Zn]_f$ at $\log_{10}[Zn]_f = -8.7$. In a Zn^{2+} sensing context, **2a** may be used for measuring $[Zn]_f$ in the nanomolar regime. Encouraged by the large fluorescence enhancement upon Zn^{2+} coordination, the satisfactory φ_f of the dizinc complex, and the nanomolar detection range suitable for $[Zn]_f$ analysis in

mammalian cellular environment,[36] **2a** was evaluated further for its potential in live-cell imaging of Zn^{2+}.

Preliminary live cell imaging study

The potential of compound **2a** as an indicator to report intracellular free Zn^{2+} status was investigated in living cells. HeLa cells were incubated in HBSS buffer in the presence of **2a** (9.5 μM) for 30 min. After replacement of media to remove the extracellular indicator molecules, the cells were incubated further in HBSS with sodium pyrithione (100 μM), a Zn^{2+} transporter for facilitating Zn^{2+} entry through cell membrane,[39] in the absence or presence of 100 μM $ZnCl_2$ for 10 min. Over the course of the experiment, no apparent toxicity of **2a** was observed based on the lack of cell morphology change.

Fluorescence images of the live cells were acquired using a Q-Max Blue filter set (Omega Filters; excitation 355–405 nm; emission 420–480 nm). When incubated under Zn^{2+}-poor conditions (Fig. 11A–B), the cells displayed weak emission. A control experiment indicates that the emission primarily originates from autofluorescence (Fig. S16†). Under zinc-enriched conditions, the fluorescence was enhanced, albeit moderately. In addition to the increase of overall intensity, cells show heightened nuclear fluorescence signals. The physiological relevance of the zinc status-dependent signal localization is currently under investigation. Because the maximal excitation of **2a** occurs in the UV range, the irradiation intensity is severely attenuated by the glass-based optical setup of the fluorescence microscope. As a result, the indicator was inefficiently excited, which led to the observed overall weak fluorescence. Although this work demonstrates the potential utility of our heteroditopic ligand system in fluorescence imaging of intracellular zinc status, it emphasizes the need for indicators that are excited with longer excitation wavelengths, as argued by many investigators for various reasons.[33]

Conclusion

A detailed study on fluorescent heteroditopic ligands **2a** and **2b** is presented. This work was motivated by the challenge to tune structural factors of the heteroditopic ligand framework (Fig. 1) to maximize the fluorescence contrast between non-, mono-, and dizinc coordinated states. We found that the electronic property of the fluorophore in the ditopic ligand exerts opposite effects on the efficiencies of PET and ICT, two photophysical processes that lead to Zn^{2+}-dependent fluorescence modulations. A ditopic ligand containing an electron-poor fluorophore (*e.g.* **2a**) may enjoy a sensitive fluorescence enhancement without much emission band shift upon binding Zn^{2+}. Increasing the electron density of the fluorophore creates a larger Zn^{2+}-induced spectral shift however with the sacrifice of fluorescence enhancement (*e.g.* in **2b**). Therefore, a delicate balance of the electronic structural features of the fluorophore in terms of the charge-transfer character and electron-accepting ability in the excited state is entailed to create a fluorescent heteroditopic system with maximum fluorescence contrast between three coordination states. In order to reduce the dependence of fluorescence contrast of various species on the electronic nature of the fluorophore, new designs of heteroditopic ligand platforms that operate under fundamentally different coordination-mediated photophysical processes are warranted.[40]

Experimental section

Materials and general methods

Reagents and solvents were purchased from various commercial sources and used without further purification unless otherwise stated. Spectroscopic grade CH_3CN was used in titration experiments. All reactions were carried out in oven- or flame-dried glassware in an

inert atmosphere of argon. Analytical thin-layer chromatography (TLC) was performed using pre-coated TLC plates with silica gel 60 F254 or with aluminium oxide 60 F254 neutral. Flash column chromatography was performed using 40–63 μm (230–400 mesh) silica gel or alumina (80–200 mesh, pH 9–10) as the stationary phases. ^{1}H and ^{13}C NMR spectra were recorded at 300 MHz and 75 MHz, respectively. All chemical shifts were reported in δ units relative to tetramethylsilane. $CDCl_3$ was treated with alumina gel prior to use.

Synthesis

Syntheses of compounds **5** and **9** were reported previously.[8,9]

Compound 3—NaH (60% in mineral oil, 4 mmol, 160 mg) was added at 0 °C to a solution of 2-pyridinecarboxaldehyde (234.6 mg, 2.18 mmol) in dry dimethoxyethane (4.0 mL) in a flamed-dried round-bottom flask. The suspension was stirred for 5 min. A solution of **5** (2.18 mmol, 703.9 mg) in dry dimethoxyethane (4.0 mL) was added dropwise to the flask with stirring at 0 °C. The stirring was continued for overnight at rt. The reaction mixture was then cooled to 0 °C before brine (2 mL) was added. The reaction mixture was stirred for another 5 min, and was partitioned between ethyl acetate (EtOAc) and water. The aqueous layer was washed with EtOAc (50 mL × 3) and the organic portions were combined. The organic portions were dried over Na_2SO_4 followed by solvent removal under vacuum. Compound **3** was isolated using silica chromatography eluted by EtOAc in CH_2Cl_2 (gradient 0–30%). The isolated yield was 75%. ^{1}H NMR (300 MHz, $CDCl_3$): δ (ppm) 8.82 (s, 1H), 8.64 (d, J = 4.3 Hz, 1H), 8.51 (s, 1H), 8.39 (d, J = 8.3 Hz, 1H), 8.31 (d, J = 8.1 Hz, 1H), 8.04 (dd, J = 8.4, 2.1 Hz, 1H), 7.68 (m, 3H), 7.42 (d, J = 7.8 Hz, 1H), 7.30 (s, 1H), 7.20 (dd, J = 4.4, 2.1 Hz, 1H), 2.41 (s, 3H). ^{13}C NMR (75 MHz, $CDCl_3$): δ (ppm) 154.6, 153.8, 152.1, 148.6, 147.6, 136.4, 135.6, 132.8, 132.4, 130.9, 128.5, 127.7, 121.5, 119.5, 17.3. HRMS (ESI+): calcd. ($C_{18}H_{15}N_3$ +H^+) 274.1344, found 274.1338.

Compound 7—2-Methylthiophene (3 mL, 30 mmol) was dissolved in CCl_4 (150 mL) and the solution was heated to reflux. Benzoyl peroxide (60 mg, 0.25 mmol) was added to the refluxing mixture. After 5 min another batch of benzoyl peroxide (60 mg, 0.25 mmol) and *N*-bromosuccinimide (5.34 g, 30 mmol) were added. The solution was refluxed for 1 h. After cooling to rt, the reaction mixture was diluted by hexanes. The precipitate was removed *via* filtration. Compound **7** was obtained upon solvent removal (5.23 g, 98%). ^{1}H NMR (300 MHz, $CDCl_3$): δ (ppm) 7.33 (d, J = 6.0 Hz, 1H), 7.12 (d, J = 3.0 Hz, 1H), 6.95 (m, 1H), 4.76 (s, 2H).

Compound 8—Compound **7** (5.23 g, 29.5 mmol) was dissolved in triethyl phosphite (10 mL). The mixture was heated at 125 °C for 4 h. The excess of triethyl phosphite was removed under high vacuum in a fume hood. The crude product was isolated by silica chromatography to afford compound **8** (6.60 g, 95%). ^{1}H NMR (300 MHz, $CDCl_3$): δ (ppm) 7.19–7.17 (m, 1H), 6.98–6.95 (m, 2H), 4.08 (m, 4H), 3.37 (d, J = 21 Hz, 2H), 1.31 (m, 6H).

Compound 10—Reaction flask was protected from ambient light using aluminium foil; work-up and purification were carried out under illumination with a red light bulb. NaH (60% in mineral oil, 0.75 mmol, 30 mg) was added at 0 °C to a solution of **9** (58.4 mg, 0.32 mmol) in dry dimethoxyethane (1.0 mL) in a flamed-dried reaction flask. The suspension was stirred for 5 min. A solution of **8** (173.1 mg, 0.73 mmol) in dry dimethoxyethane (1.0 mL) was added dropwise to the reaction flask with stirring at 0 °C. The stirring was continued overnight at rt. The reaction mixture was then cooled to 0 °C before brine (1 mL) was added. The reaction mixture was stirred for another 5 min, and was partitioned between CH_2Cl_2 and basic brine. The aqueous layer was washed with CH_2Cl_2 (50 mL × 3) and the

organic portions were combined. The organic portions were dried over Na_2SO_4 followed by solvent removal under vacuum. The residue was purified by silica column to afford compound **10** (21.0 mg, 25%). ^{1}H NMR (300 MHz, $CDCl_3$): δ (ppm) 7.19 (d, J = 4.8 Hz, 1H), 7.05–7.68 (m, 5H), 6.92 (d, J = 3.3 Hz, 1H), 6.08 (s, 1H), 4.18–4.01 (m, 4H); ^{13}C NMR (75 MHz, $CDCl_3$): δ (ppm) 143.5, 142.4, 140.6, 127.8, 126.9, 126.4, 125.7, 124.7, 122.1, 121.6, 100.5, 65.4; HRMS (EI+): calcd. ($C_{13}H_{12}O_2S_2 + H^+$) 264.0279, found 264.0281.

Compound 11—Reaction flask was protected from ambient light using aluminium foil; work-up and purification were carried out under illumination with a red light bulb. Compound **10** (21 mg, 0.08 mmol) was dissolved in a mixed solvent (5 mL) of 37% HCl–H_2O–THF (1 : 6 : 7). The solution was stirred overnight before being partitioned between basified brine (pH > 11) and CH_2Cl_2 (3 × 50 mL). The organic portions were dried over Na_2SO_4 before concentration under vacuum. The purity of the product judging by TLC and NMR (^{1}H and ^{13}C) spectra is sufficient for the next step. The yield was quantitative. ^{1}H NMR (300 MHz, $CDCl_3$): δ (ppm) 9.86 (s, 1H), 7.66 (d, J = 4.2 Hz, 1H), 7.31–7.26 (m, 2H), 7.16 (d, J = 3.6 Hz, 1H), 7.12 (d, J = 4.2 Hz, 1H), 7.05 (t, J = 1.8 Hz, 1H), 7.01 (d, J = 9.6 Hz, 1H); ^{13}C NMR (75 MHz, $CDCl_3$): δ (ppm) 182.6, 152.2, 141.6, 141.5, 137.4, 128.3, 128.2, 126.6, 126.4, 126.0, 120.4; HRMS (ESI+): calcd. ($C_{11}H_8OS_2 + Na^+$) 242.9914, found 242.9913.

Compound 4—Reaction flask was protected from ambient light using aluminium foil; work-up and purification were carried out under illumination with a red light bulb. NaH (60% in mineral oil, 0.4 mmol, 16 mg) was added at 0 °C to a solution of **11** (21.3 mg, 0.09 mmol) in dry dimethoxyethane (0.5 mL) in a flamed-dried reaction flask. The suspension was stirred for 5 min. A solution of **5** (32 mg, 0.10 mmol) in dry dimethoxyethane (0.5 mL) was added dropwise to the reaction flask with stirring at 0 °C. The stirring was continued overnight at rt. The reaction mixture was then cooled to 0 °C before brine (1 mL) was added. The reaction mixture was stirred for another 5 min, and was partitioned between CH_2Cl_2 and basified brine (pH > 11). The aqueous layer was washed with CH_2Cl_2 (20 mL × 3) and the organic portions were combined. The organic portions were dried over Na_2SO_4 followed by solvent removal under vacuum. The residue was purified using silica chromatography eluted by EtOAc in CH_2Cl_2 (gradient 0–15%). The isolated product (34.3 mg, 92%) was further purified by precipitation from a CH_2Cl_2 solution by addition of hexanes to afford pure compound **4** (18.9 mg, 51%). ^{1}H NMR (300 MHz, $CDCl_3$): δ (ppm) 8.62 (s, 1H), 8.43 (s, 1H), 8.27 (d, J = 8.3 Hz, 1H), 8.22 (d, J = 8.1 Hz, 1H), 7.82 (dd, J = 2.1, 8.4 Hz, 1H), 7.54 (d, J = 8.3 Hz, 1H), 7.23–7.12 (m, 3H), 6.91 (m, 6H), 2.32 (s, 3H). ^{13}C NMR (75 MHz, $CDCl_3$): δ (ppm) 149.9, 148.1, 142.5, 142.4, 141.4, 137.6, 133.6, 133.3, 132.6, 128.3, 127.9, 127.3, 126.6, 124.9, 124.7, 123.9, 122.3, 121.5, 120.9, 120.8, 18.6. HRMS (ESI+): calcd. ($C_{23}H_{18}N_2S_2$+H^+) 387.0990, found 387.0995.

Compound 12—Reaction flask was protected from ambient light using aluminium foil; work-up and purification were carried out under illumination with a red light bulb. NaH (60% in mineral oil, 15 mmol, 600 mg) was added at 0 °C to a solution of 2-thiophenecarboxaldehyde (4.3 mmol, 400 μL) in dry dimethoxyethane (5 mL) in a flamed-dried reaction flask. The suspension was stirred for 10 min. A solution of **8** (2 g, 4.23 mmol) in dry dimethoxyethane (5 mL) was added dropwise to the reaction flask with stirring at 0 °C. The stirring was continued overnight at rt. The reaction mixture was then cooled to 0 °C before brine (10 mL) was added. The reaction mixture was stirred for another 5 min, and was partitioned between CH_2Cl_2 and water. The aqueous layer was washed with CH_2Cl_2 (50 mL × 3) and the organic portions were combined. The organic portions were dried over Na_2SO_4 followed by solvent removal under vacuum. The residue was purified by silica column to afford pure **12** (722 mg, 88%). ^{1}H NMR (300 MHz, $CDCl_3$): δ (ppm) 7.16 (d, J =

8.0 Hz, 2H), 7.48 (m, 4H), 7.0 (m, 2H); ^{13}C NMR (75 MHz, $CDCl_3$): δ (ppm) 142.6, 127.9, 126.2, 124.5, 121.7.

Compound 13b—$POCl_3$ (1.5 mL) was added dropwise into a solution of compound **12** (300 mg, 1.56 mmol) in DMF (1.5 mL) in a flamed-dried reaction flask at 0 °C. During the addition, the temperature was kept below 10 °C, after which the mixture was stirred for 30 min at rt before being heated at 90–95 °C for 45 min. After cooling down, the mixture was poured into crushed ice (50 mL), and made weakly alkaline with a NaOH solution (1 M). After partitioned between CH_2Cl_2 and water, the organic layer was dried over Na_2SO_4. The solvent was removed under vacuum and the residue was chromatographed (silica, hexanes–CH_2Cl_2 from 2 : 1 to 1 : 2) to afford compound **13b** (381 mg, 98%). ^{1}H NMR (300 MHz, $CDCl_3$): δ (ppm) 9.89 (s, 2H), 7.69 (d, J = 4.0 Hz, 2H), 7.24 (m, 4H); ^{13}C NMR (75 MHz, $CDCl_3$): δ (ppm) 182.8, 150.4, 143.0, 137.2, 128.4, 124.7.

Compound 14b—A round-bottom flask charged with **13b** (154 mg, 0.62 mmol) and ethylene glycol (35 μL, 0.62 mmol) in benzene (12 mL) was equipped with a Dean–Stark tube (5 mL). Catalytic amount of TsOH was added and the reaction mixture was stirred for 5 h under reflux. After the reaction mixture was cooled to rt, solvent was removed and the residue was partitioned between CH_2Cl_2 and a $NaHCO_3$ solution (0.1 M). The organic portion was separated and dried over Na_2SO_4 before solvent was removed under vacuum. The crude product was chromatographed (silica, hexanes–CH_2Cl_2 from 1 : 1 to 1 : 9) to afford a mixture of compound **14b** and starting material, which was used directly to the next step.

Compound 15b—Reaction flask was protected from ambient light using aluminium foil; work-up and purification were carried out under illumination with a red light bulb. Di-(2-picolyl)amine (51 μL) was added dropwise into a 1,2-dichloroethane (2.3 mL) solution of **14b** from the previous step (80 mg). The reaction mixture was stirred overnight before the addition of sodium triacetoxyborohydride (183 mg, 0.86 mmol). The mixture was stirred for another 2 h before the solvent was removed under vacuum. The residue was washed with basified brine (pH = 11) and extracted with CH_2Cl_2 (3 × 25 mL). The organic portions were dried over K_2CO_3 before being concentrated under vacuum. Compound **15b** (38 mg) was isolated by alumina chromatography (CH_2Cl_2–EtOAc from 10 : 1 to 1 : 1). ^{1}H NMR (300 MHz, $CDCl_3$) δ (ppm) 8.52 (d, J = 3.0 Hz, 2H), 7.72–7.65 (m, 4H), 7.19–7.15 (m, 2H), 7.03 (d, J = 3.0 Hz, 1H), 6.96 (s, 2H), 6.90 (d, J = 3.0 Hz, 1H), 6.87–6.84 (m, 2H), 6.05 (s, 1H), 4.15 (m, 2H), 4.05 (m, 2H), 3.85 (s, 6H); ^{13}C NMR (75 MHz, $CDCl_3$): δ (ppm) 159.6, 149.1, 144.5, 140.8, 136.8, 126.2, 125.6, 122.9, 122.3, 100.7, 65.4, 59.9, 53.5; HRMS (ESI +): calcd. ($C_{26}H_{25}N_3O_2S_2 + Na^+$) 498.1286, found 498.1272.

Compound 16b—Reaction flask was protected from ambient light using aluminium foil; work-up and purification were carried out under illumination with a red light bulb. Compound **15b** (38 mg, 0.08 mmol) was dissolved in a mixed solvent (10 mL) of 37% HCl–H_2O–THF (1 : 6 : 7). The solution was stirred overnight before partitioned using basified brine (pH = 11) and CH_2Cl_2 (3 × 25 mL). The organic portions were dried over K_2CO_3 before being concentrated under vacuum. The crude compound **16b** (34 mg, 100%) was pure enough to use in the next step. ^{1}H NMR (300 MHz, $CDCl_3$): δ (ppm) 9.85 (s, 1H), 8.53 (d, J = 4.8 Hz, 2H), 7.67–7.65 (m, 4H), 7.25–7.16 (m, 4H), 7.11 (d, J = 3.6 Hz, 1H), 7.00 (d, J = 4.2 Hz, 1H), 6.96 (d, J = 7.8 Hz, 1H), 6.88 (d, J = 3.0 Hz, 1H), 3.87 (s, 4H), 3.85 (s, 2H). ^{13}C NMR (75 MHz, $CDCl_3$): δ (ppm) 182.6, 159.5, 149.3, 144.8, 141.6, 140.9, 137.4, 136.8, 128.3, 127.1, 126.4, 126.3, 123.0, 122.4, 119.9, 59.9, 53.5; HRMS (ESI+): calcd. ($C_{24}H_{21}N_3OS_2 + Na^+$) 454.1024, found 454.1016.

Compound 2b—Reaction flask was protected from ambient light using aluminium foil; work-up and purification were carried out under illumination with a red light bulb. NaH (60% in mineral oil, 14 mg, 0.35 mmol) was added to a solution of **16b** (37.4 mg, 0.09 mmol) in anhydrous dimethoxyethane (0.5 mL) in the reaction flask. The suspension was stirred for 8 min. The flask was cooled in an ice bath (0 °C) and a solution of **5** (28 mg, 0.09 mmol) in anhydrous dimethoxyethane (0.5 mL) was added dropwise. The reaction was stirred overnight before icy brine was added to quench the reaction. The reaction mixture was partitioned between CH_2Cl_2 and basified brine (pH = 11). The organic layer was dried over Na_2SO_4, followed by solvent removal under vacuum. The residue was chromatographed on alumina gel by using 10% EtOAc in CH_2Cl_2. The isolated product (41.1 mg, 76%) was precipitated from a CH_2Cl_2 solution by addition of hexanes to afford pure *trans*-**2b** (6.4 mg, 12%). ^{1}H NMR (300 MHz, $CDCl_3$): δ (ppm) 8.69 (s, 1H), 8.54–8.50 (m, 3H), 8.34 (d, J = 8.1 Hz, 1H), 8.29 (d, J = 8.0 Hz, 1H), 7.91 (d, J = 8.3 Hz, 1H), 7.74–7.61 (m, 5H), 7.29 (2H), 7.17 (t, J = 5.3 Hz, 2H), 7.01–3.86 (m, 7H), 3.86 (s, 6H), 2.40 (s, 2H). ^{13}C NMR (75 MHz, $CDCl_3$): δ (ppm) 159.6, 155.2, 149.9, 149.2, 148.1, 141.9, 137.7, 136.8, 133.3, 128.4, 127.1, 126.9, 124.5, 123.9, 122.9, 122.7, 122.3, 121.0, 120.9, 120.8, 59.9, 53.6, 18.6. HRMS (ESI+): calcd. ($C_{36}H_{31}N_5S_2 + H^+$) 598.2099, found 598.2086.

Compound 14a—A round-bottom flask charged with 2,6-pyridinedicarboxaldehyde (590.4 mg, 4.37 mmol) and ethylene glycol (243 μL, 4.35 mmol) in benzene (22 mL) was equipped with a Dean–Stark tube (5 mL). Catalytic amount of TsOH was added and the reaction mixture was stirred for 5 h under reflux. After the reaction mixture was cooled to rt, solvent was removed and the residue was partitioned between CH_2Cl_2 and $NaHCO_3$ (0.1 M). The organic portion was separated and dried over Na_2SO_4 before solvent was removed under vacuum. The crude product was chromatographed (silica, CH_2Cl_2) to afford **14a** (152.6 mg, 20%). ^{1}H NMR (300 MHz, $CDCl_3$): δ (ppm) 10.12 (s, 1H), 7.98 (d, J = 5.4 Hz, 1H), 7.95 (d, J = 5.4 Hz, 1H), 7.79 (dd, J = 1.8, 7.2 Hz, 1H), 5.95 (s, 1H), 4.25–4.11 (m, 4H); ^{13}C NMR (75 MHz, $CDCl_3$): δ (ppm) 193.4, 158.1, 152.5, 138.1, 125.1, 121.8, 103.3, 65.9.

Compound 15a—Di-(2-picolyl)amine (76 μL, 0.42 mmol) was added dropwise into a 1,2-dichloroethane (3 mL) solution of **14a** (55 mg, 0.30 mmol). The reaction mixture was stirred overnight before the addition of sodium triacetoxyborohydride (260 mg, 1.23 mmol). The reaction mixture was stirred for another 6 h. Brine (1 mL) was added to quench the reaction. The reaction mixture was diluted with water and carefully basified to pH 11. The basified aqueous portion was extracted with CH_2Cl_2 (50 mL × 3). The organic portions were combined and dried over K_2CO_3. The solvent was removed and the residue was chromatographed on alumina gel by using 10% EtOAc in CH_2Cl_2 to afford **15a** (63.1 mg, 58%). ^{1}H NMR (300 MHz, $CDCl_3$): δ (ppm) 8.53 (d, J = 4.8 Hz, 2H), 7.21–7.57 (m, 6H), 7.41 (d, J = 7.8 Hz, 1H), 7.16–7.13 (m, 2H), 5.83 (s, 1H), 4.20–4.06 (m, 4H), 3.92 (s, 2H), 3.89 (s, 4H); ^{13}C NMR (75 MHz, $CDCl_3$): δ (ppm) 159.5, 159.4, 156.5, 149.2, 137.3, 136.5, 123.1, 123.1, 122.1, 118.8, 103.9, 65.6, 60.3, 60.2; HRMS (ESI+): calcd. ($C_{21}H_{22}N_4O_2 + Na^+$) 385.1640, found 385.1627.

Compound 16a—Compound **15a** (63 mg, 0.17 mmol) was dissolved in a mixed solvent (5 mL) of 37% HCl–H_2O–THF (1 : 6 : 7). The solution was stirred for 3 days before partitioned using basified brine (pH = 11) and CH_2Cl_2 (3 × 25 mL). The organic portions were dried over K_2CO_3 before concentrated under vacuum. The residue was chromatographed (alumina, CH_2Cl_2–EtOAc from 10 : 1 to 1 : 1) to afford **16a** (21.6 mg, 40%). ^{1}H NMR (300 MHz, $CDCl_3$): δ (ppm) 10.04 (s, 1H), 8.54 (d, J = 4.2 Hz, 2H), 7.82 (s, 2H), 7.69–7.54 (m, 5H), 7.18–7.13 (m, 2H), 4.00 (s, 2H), 3.93 (s, 4H).

Compound 2a—Reaction flask was protected from ambient light using aluminium foil; work-up and purification were carried out under illumination with a red light bulb. NaH (60% in mineral oil, 11 mg, 0.28 mmol) was added to a solution of **16a** (21.6 mg, 0.067 mmol) in anhydrous dimethoxyethane (0.5 mL) in the reaction flask. The suspension was stirred for 8 min. The flask was cooled in an ice bath (0 °C) and a solution of **3** (30.3 mg, 0.09 mmol) in anhydrous dimethoxyethane (0.5 mL) was added dropwise. The reaction was stirred overnight before icy brine was added to quench the reaction. The reaction mixture was partitioned between CH_2Cl_2 and basified brine (pH = 11). The organic layer was dried over Na_2SO_4, followed by solvent removal under vacuum. The residue was chromatographed on alumina gel by using 10% EtOAc in CH_2Cl_2. The isolated product was precipitated from a CH_2Cl_2 solution by addition of hexanes to afford pure *trans*-**2a** (14.9 mg, 46%). ^{1}H NMR (300 MHz, $CDCl_3$): δ (ppm) 8.81 (d, J = 1.8 Hz, 1H), 8.55 (d, J = 4.8 Hz, 1H), 8.52 (s, 1H), 8.38 (d, J = 8.4 Hz, 1H), 8.31 (d, J = 8.4 Hz, 1H), 8.02 (dd, J = 1.8, 8.4 Hz, 1H), 7.71–7.63 (m, 7H), 7.50 (d, J = 7.8 Hz, 1H), 7.29–7.18 (m, 3H), 7.18–7.14 (m, 2H), 3.95 (s, 6H), 2.41 (s, 3H); ^{13}C NMR (75 MHz, $CDCl_3$): δ (ppm) 159.8, 155.9, 154.6, 153.6, 145.0, 149.4, 148.8, 137.6, 137.2, 136.6, 134.2, 133.7, 132.4, 130.3, 129.0, 123.2, 122.2, 121.9, 120.9, 120.9, 120.8, 60.5, 60.5, 18.6; HRMS (ESI+): calcd. ($C_{31}H_{28}N_6$ + Na^+) 507.2273, found 507.2255.

X-Ray crystallography

A very irregular crystal of **2b** was mounted on a nylon loop with the use of heavy oil. The sample was held at −120 °C for data collection. Full data were taken on a Bruker SMART APEX diffractometer using a detector distance of 5 cm. The number of frames taken was 2400 using 0.3 degree omega scans with 20 s of frame collection time with a final 50 frames taken to check for decomposition. Only crystals that exhibited non-mereohedral twinning were found. The data were indexed using CELL_NOW and integrated using the program SAINT which is part of the Bruker suite of programs. Absorption corrections and the preparation of HKL4 and HKL5 files were done using TWINABS. XPREP was used to obtain an indication of the space group and the structure was solved by direct methods and refined by SHELXTL. The non hydrogen atoms were refined anisotropically and the hydrogens were assigned as a riding model. Owing to the small size of the best crystal that could be found, reflections were not found at as high an angle as we would have liked.‡

Supplementary Material

Refer to Web version on PubMed Central for supplementary material.

Acknowledgments

This work was supported, in part, by a New Investigator Research grant from the James and Esther King Biomedical Research Program administered by the Florida Department of Health (08KN-16), National Science Foundation (CHE-0809201), and National Institute of General Medical Sciences (R01GM-081382). The authors also thank Chris Murphy at NHMFL for assistance in live cell fluorescence imaging experiments.

Notes and references

1. Lakowicz, JR. Principles of Fluorescence Spectroscopy. Vol. 19. Springer; 2006. Fluorescence Sensing

‡Crystallographic data of **2b**: C_{36} H_{31} N_5 S_2, MW = 597.78, Triclinic, $P\bar{1}$ (Z = 2), a = 6.2947(10) Å, b = 9.8820(12) Å, c = 25.1671(19) Å, α = 86.318(5)°, β = 83.519(6)°, γ = 81.658(7)°, V = 1537.2(3) Å^3, T = 153 K, 2148 unique reflections, Observed data with $I > 2\sigma(I)$ = 2091, R_1 =0.0378, wR_2 = 0.0996.

2. Valeur, B. Molecular Fluorescence. Principles and Applications. Vol. 10. Wiley-VCH; 2002. Fluorescent Molecular Sensors of Ions and Molecules
3. de Silva AP, Gunaratne HQN, Gunnlaugsson T, Huxley AJM, McCoy CP, Rademacher JT, Rice TE. Chem Rev. 1997; 97:1515–1566. [PubMed: 11851458]
4. Anslyn EV. Tetrahedron. 2004; 60:11055–11056.
5. de Silva AP, Tecilla P. J Mater Chem. 2005; 15:2637–2639.
6. Zhang L, Murphy CS, Kuang G-C, Hazelwood KL, Constantino MH, Davidson MW, Zhu L. Chem Commun. 2009:7408–7410.
7. Zhu L, Zhang L, Younes AH. Supramol Chem. 2009; 21:268–283.
8. Zhang L, Clark RJ, Zhu L. Chem–Eur J. 2008; 14:2894–2903. [PubMed: 18232042]
9. Zhang L, Zhu L. J Org Chem. 2008; 73:8321–8330. [PubMed: 18850742]
10. Younes AH, Zhang L, Clark RJ, Zhu L. J Org Chem. 2009; 74:8761–8772. [PubMed: 19852467]
11. de Silva AP, Moody TS, Wright GD. Analyst. 2009; 134:2385–2393. [PubMed: 19918605]
12. Mallegol T, Gmouh S, Meziane MAM, Blanchard-Desce M, Mongin O. Synthesis. 2005; 11:1771–1774.
13. Zhang L, Whitfield WA, Zhu L. Chem Commun. 2008:1880–1882.
14. Newkome GR, Nayak A, Fronczek F, Kawato T, Taylor HCR, Meade L, Mattice W. J Am Chem Soc. 1979; 101:4472–4477.
15. Hanan GS, Lehn J-M, Kyritsakas N, Fischer J. J Chem Soc, Chem Commun. 1995:765–766.
16. Jouvenot D, Glazer EC, Tor Y. Org Lett. 2006; 8:1987–1990. [PubMed: 16671763]
17. Parson, WW. Modern Optical Spectroscopy: With Examples from Biophysics and Biochemistry. Springer-Verlag; Berlin Heidelberg: 2007.
18. Valeur, B. Molecular Fluorescence Principles and Applications. Wiley-VCH; 2002.
19. Michaels HA, Murphy CS, Clark RJ, Davidson MW, Zhu L. Inorg Chem. 2010; 49:4278–4287. [PubMed: 20369825]
20. Reichardt, C. Solvents and Solvent Effects in Organic Chemistry. VCH; Weinheim: 1988.
21. Suppan, P.; Ghoneim, N. Solvatochromism. The Royal Society of Chemistry; 1997.
22. Ravi M, Samanta A, Radhakrishnan TP. J Phys Chem. 1994; 98:9133–9136.
23. Ravi M, Samanta A, Radhakrishnan TP. J Chem Soc, Faraday Trans. 1995; 91:2739–2742.
24. Sinkeldam RW, Tor Y. Org Biomol Chem. 2007; 5:2523–2528. [PubMed: 18019524]
25. Butler RS, Cohn P, Tenzel P, Abboud KA, Castellano RK. J Am Chem Soc. 2009; 131:623–633. [PubMed: 19113848]
26. de Silva AP, de Silva SA, Dissanayake AS, Sandanayake KRAS. J Chem Soc, Chem Commun. 1989:1054–1056.
27. de Silva AP, Gunaratne HQN, Lynch PLM. J Chem, Soc, Perkin Trans. 1995; 2:685–690.
28. Ueno T, Urano Y, Setsukinai K-i, Takakusa H, Kojima H, Kikuchi K, Ohkubo K, Fukuzumi S, Nagano T. J Am Chem Soc. 2004; 126:14079–14085. [PubMed: 15506772]
29. Patton C, Thompson S, Epel D. Cell Calcium. 2004; 35:427–431. [PubMed: 15003852]
30. Jiang P, Guo Z. Coord Chem Rev. 2004; 248:205–229.
31. Kikuchi K, Komatsu H, Nagano T. Curr Opin Chem Biol. 2004; 8:182–191. [PubMed: 15062780]
32. Dai Z, Canary JW. New J Chem. 2007; 31:1708–1718.
33. Que EL, Domaille DW, Chang CJ. Chem Rev. 2008; 108:1517–1549. [PubMed: 18426241]
34. Nolan EM, Lippard SJ. Acc Chem Res. 2009; 42:193–203. [PubMed: 18989940]
35. Huang S, Clark RJ, Zhu L. Org Lett. 2007; 9:4999–5002. [PubMed: 17956110]
36. Krę,żel A, Maret W. JBIC, J Biol Inorg Chem. 2006; 11:1049–1062.
37. Bozym RA, Thompson RB, Stoddard AK, Fierke CA. ACS Chem Biol. 2006; 1:103–111. [PubMed: 17163650]
38. Fahrni CJ, O'Halloran TV. J Am Chem Soc. 1999; 121:11448–11458.
39. Forbes IJ, Zalewski PD, Hurst NP, Giannakis C, Whitehouse MW. FEBS Lett. 1989; 247:445–447. [PubMed: 2785460]

40. See a preliminary study on a new heteroditopic design: Wandell RJ, Younes AH, Zhu L. New J Chem. 201010.1039/c0nj00241k

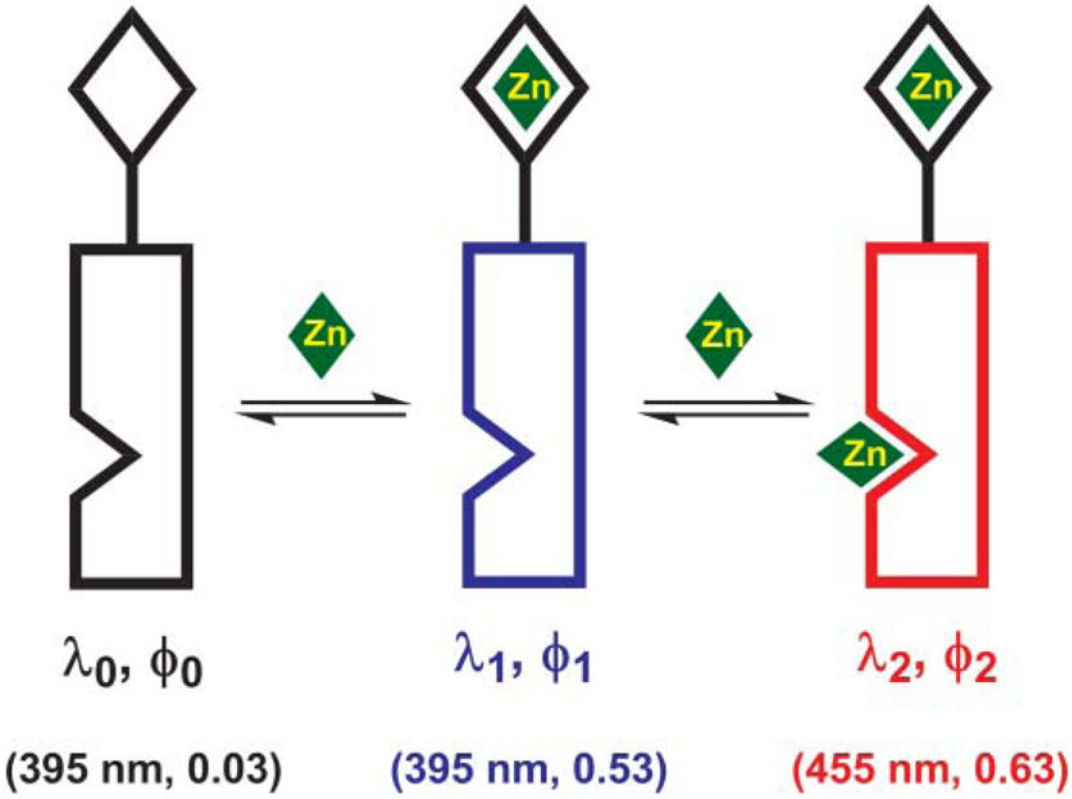

Fig. 1.

An illustration showing the fluorescent heteroditopic ligand and its three coordination states. Diamond on top: high-affinity Zn^{2+} binding site, also the electron donor in photoinduced electron transfer (PET). Nicked rectangle: the fluorophore which contains the low-affinity Zn^{2+} binding site, shown as the nick. λ – emission wavelength; φ – fluorescence quantum yield; subscripts denote the coordination status. The relevant values of compound **1** in CH_3CN are listed in the parentheses.

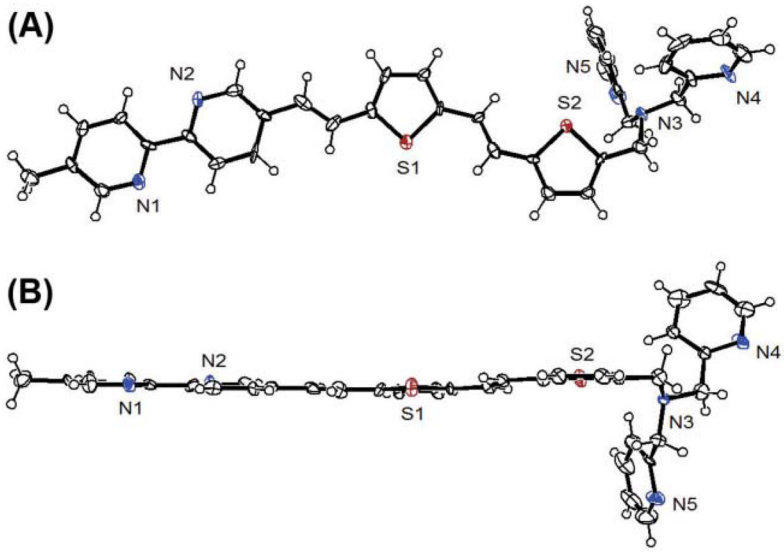

Fig. 2.

Two views of the X-ray crystal structure of **2b** (50% probability ellipsoids). The heteroatoms are labelled.

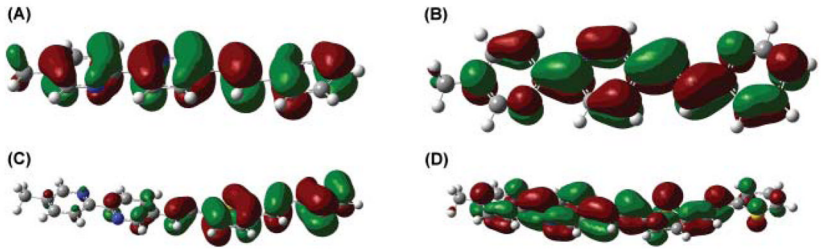

Fig. 3.
(A) HOMO of **3**, (B) LUMO of **3**, (C) HOMO of **4**, and (D) LUMO of **4** calculated at B3LYP/6-31+G(d,p) level of theory.

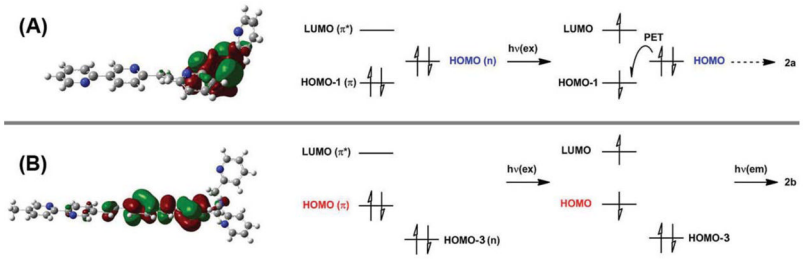

Fig. 4.

Left: HOMO diagrams of **2a** (A) and **2b** (B). Right: illustrations of frontier molecular orbital arrangements during photoexcitation of **2a** (A) and **2b** (B). The orbital diagrams of other frontier orbitals are shown in Figures S5–S6†. hν(ex): photons in excitation; hν(em): emitted photon. PET: photoinduced electron transfer. Solid arrows: radiative processes; dashed arrow: nonradiative process.

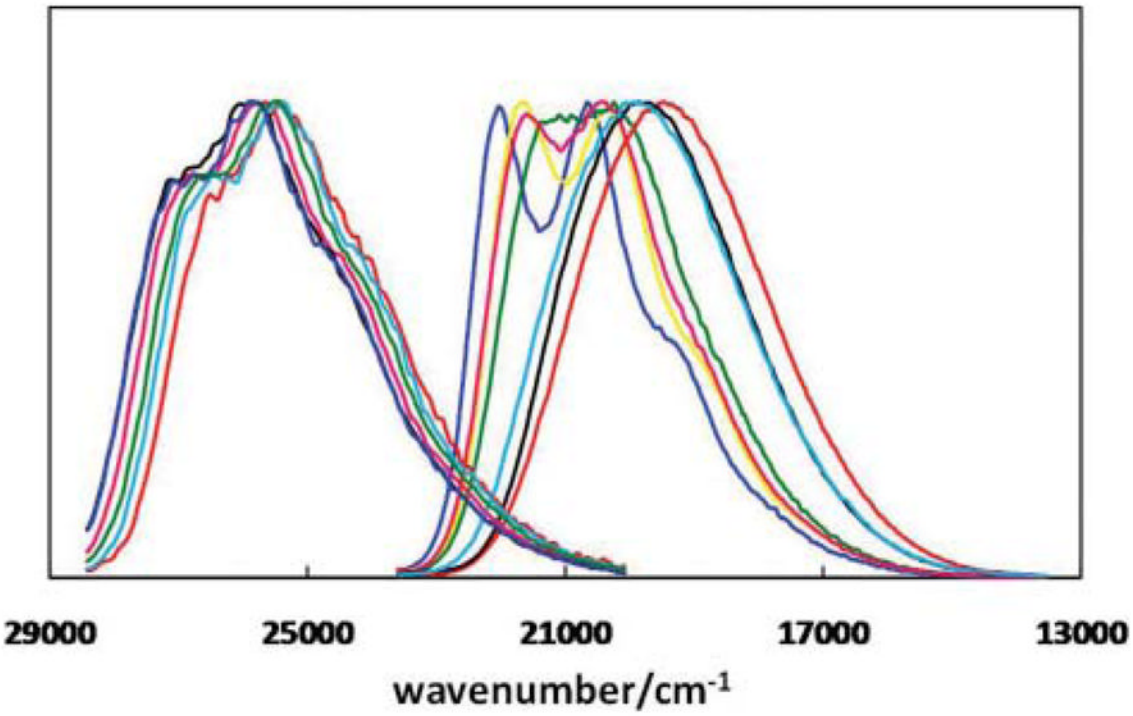

Fig. 5.

Normalized emission spectra of **3** (clustered on the left) and **4** (right) in various solvents. For the spectra of **4**, the colour coding from left to right is the following: blue – cyclohexane (ε = 2.0), yellow – benzene (ε = 2.3), pink – dioxane (ε = 2.2), green – chloroform (ε = 4.8), cyan – DMSO (ε = 46.4), black – acetonitrile (ε = 35.9), and red – methanol (ε = 32.7). ε: relative permittivity.[20]

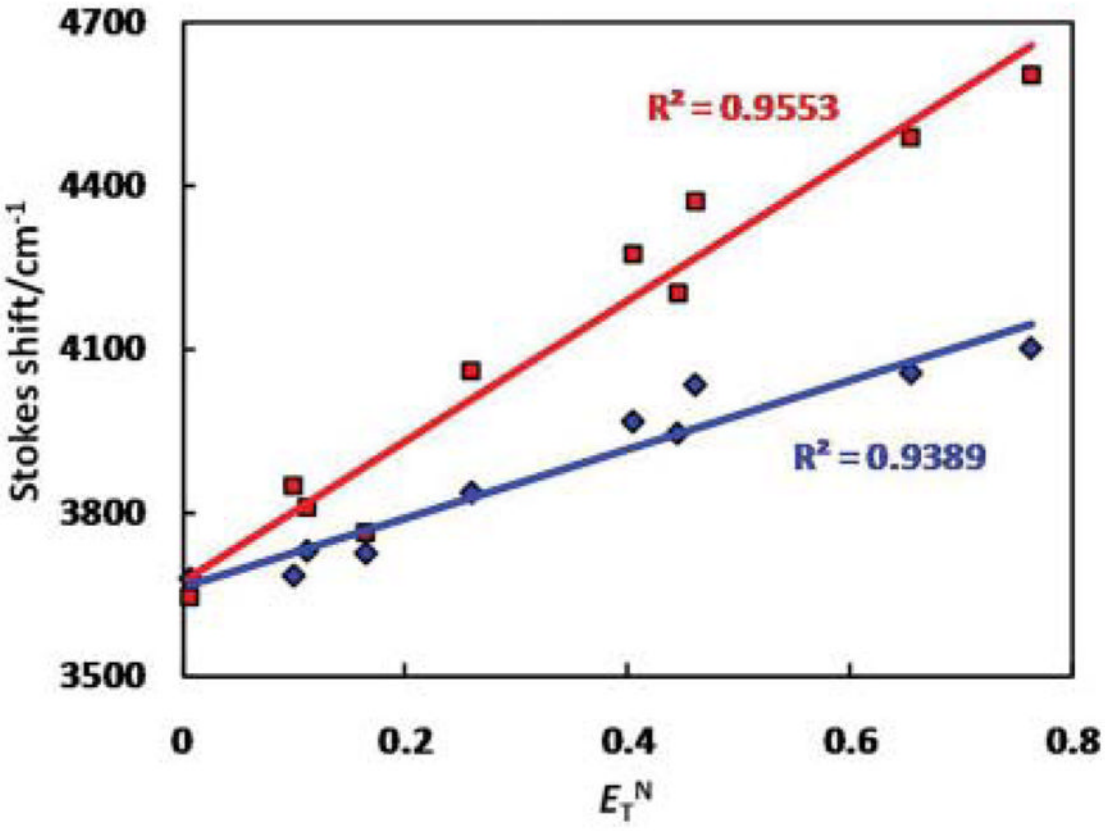

Fig. 6.
Modified Lippert plots of compounds **3** (blue) and **4** (red). $E_T{}^N$: normalized Reichardt's E_T (30) solvent parameter.

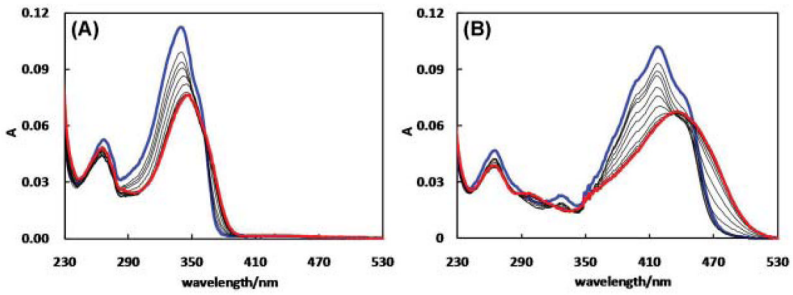

Fig. 7.

Absorption spectra of (A) **2a** (2.9 μM) in CH_3 CN upon addition of $ZnCl_2$ (0–26 μM) and (B) **2b** (1.9 μM) in CH_3 CN upon addition of $ZnCl_2$ (0–14 μM). The spectra that were collected at the beginning and the end of a titration experiment are coded blue and red, respectively.

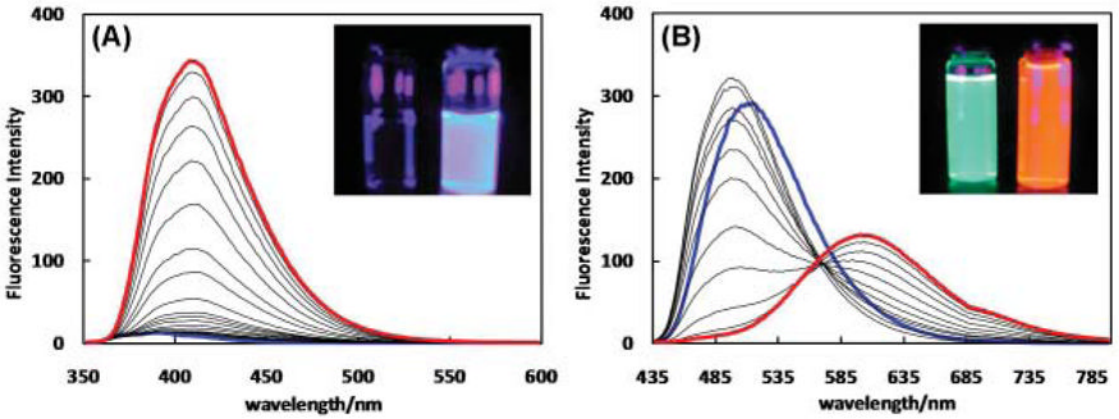

Fig. 8.

Emission spectra of (A) **2a** (2.9 μM) in CH_3 CN (λ_{ex} = 340 nm) upon addition of $ZnCl_2$ (0–33 μM) and (B) **2b** (1.9 μM) in CH_3 CN (λ_{ex} = 430 nm) upon addition of $ZnCl_2$ (0–51 μM). The spectra that were collected at the beginning and the end of a titration experiment are coded blue and red, respectively.

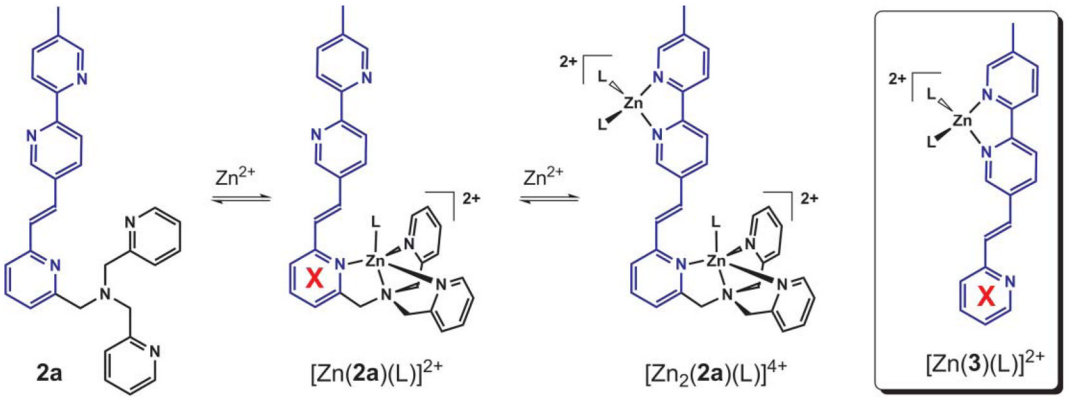

Fig. 9.

Three coordination states of **2a** along a Zn^{2+} gradient. L: coordinating solvent. Note that Zn^{2+} resides at different ends of the fluorophore in the monozinc complexes of **2a** and **3**. The red crosses highlight the difference in coordination status of this pyridyl group in the monozinc complexes of ditopic **2a** and monotopic **3**.

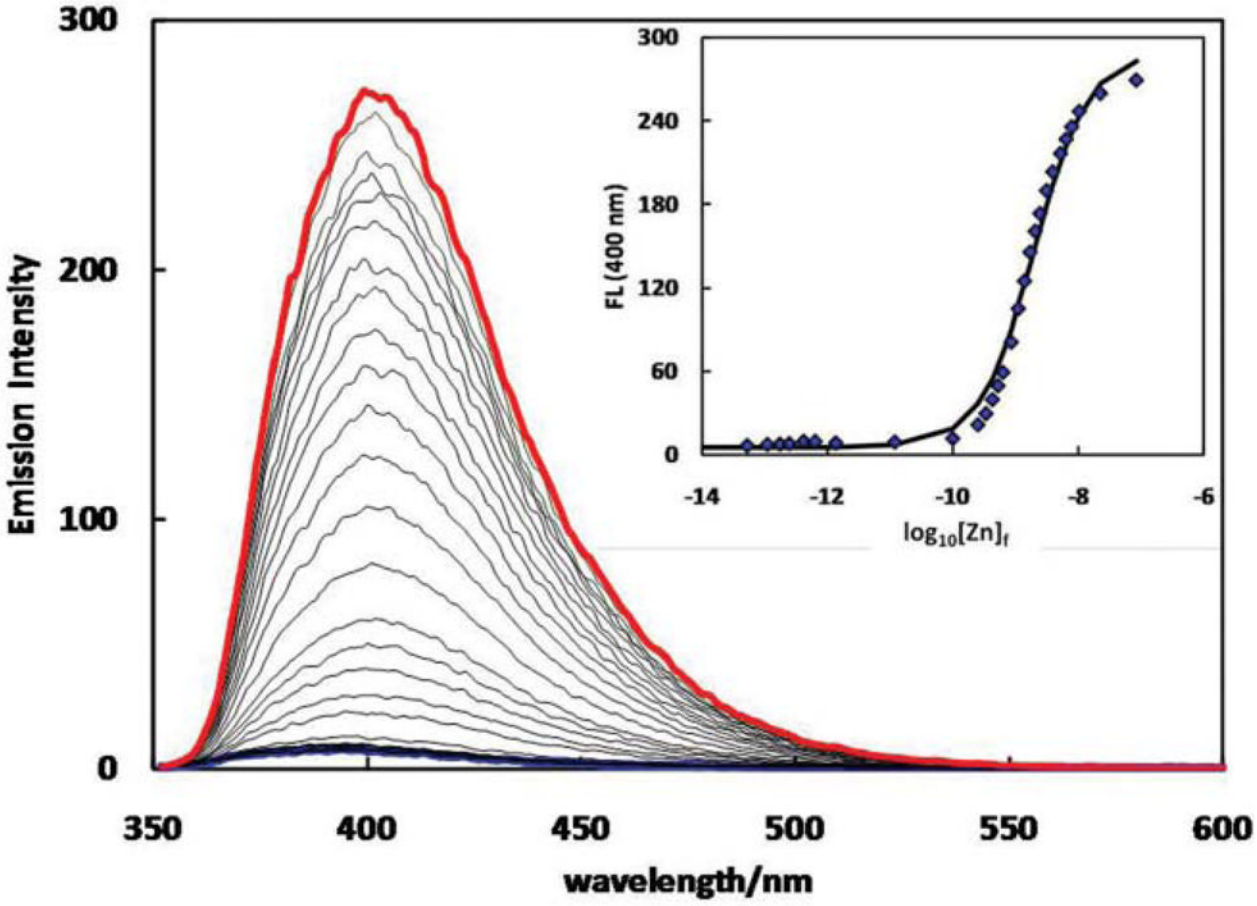

Fig. 10.

Emission spectra of **2a** (6.4 μM, λ_{ex} = 340 nm) in 10% DMSO-containing aqueous solution (HEPES: 50 mM, pH = 7.4, HEDTA: 2.5 mM, EGTA: 2.5 mM, NTA: 5 mM, KNO_3: 100 mM) upon addition of $Zn(ClO_4)_2$ (0–8.8 mM). The spectra that were collected at the beginning and the end of a titration experiment are coded blue and red, respectively. Inset: fluorescence intensity at 400 nm *vs.* $\log_{10}[Zn]_f$ ($[Zn]_f$ – free zinc ion concentration, calculated using "Webmaxc Standard"[6,29]).

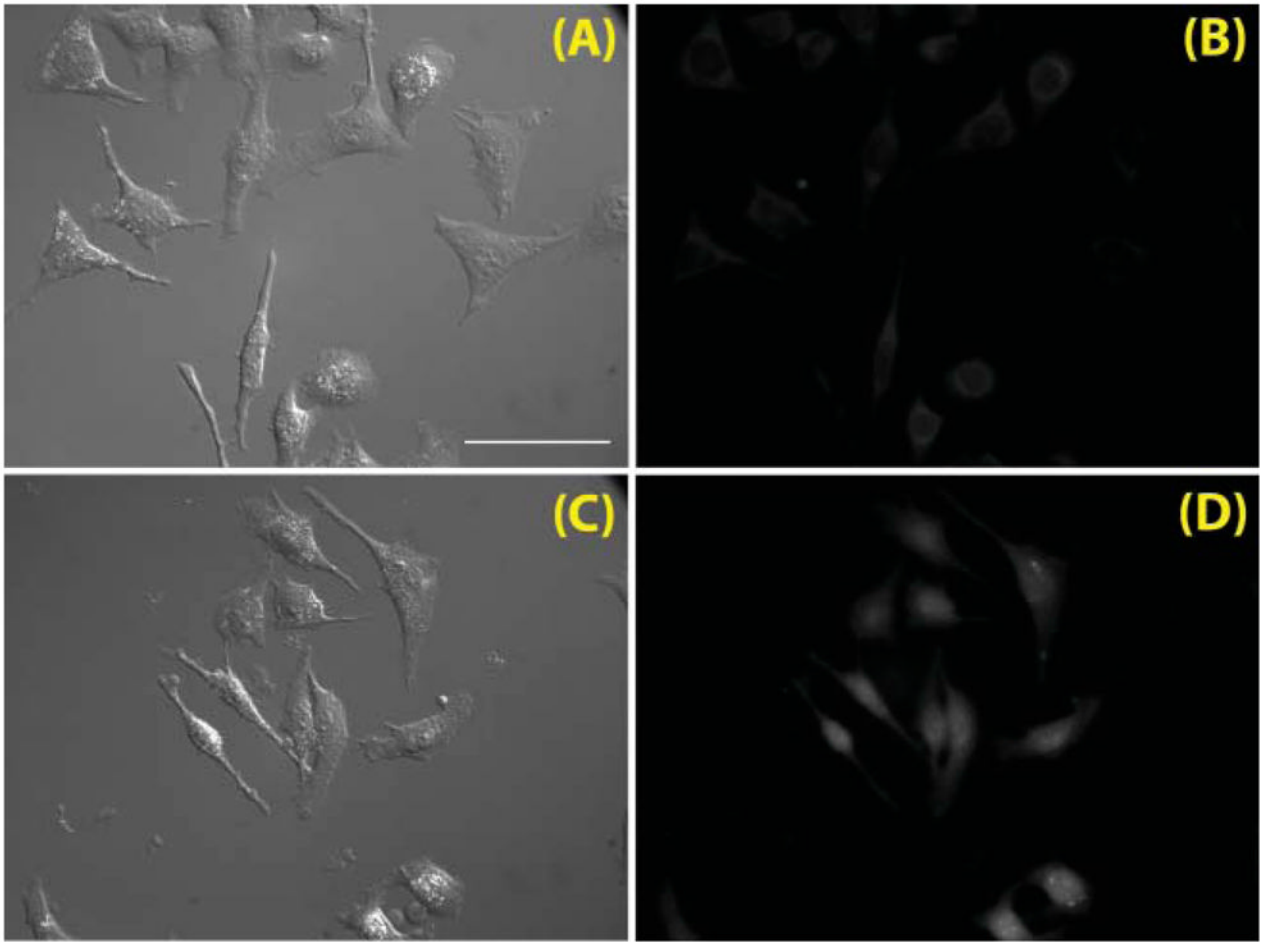

Fig. 11.

(A) Differential interference contrast (DIC) and (B) fluorescence images (Omega Q-Max Blue filter set; excitation 355–405 nm; emission 420–480 nm) of live HeLa cells loaded with **2a** (incubation time 30 min, loading concentration 9.5 μM) in HBSS buffer at 37 °C under 5% CO_2. (C) DIC and (D) fluorescence images of live HeLa cells treated under the same conditions in the presence of 100 μM $ZnCl_2$. Scale bar – 50 μm.

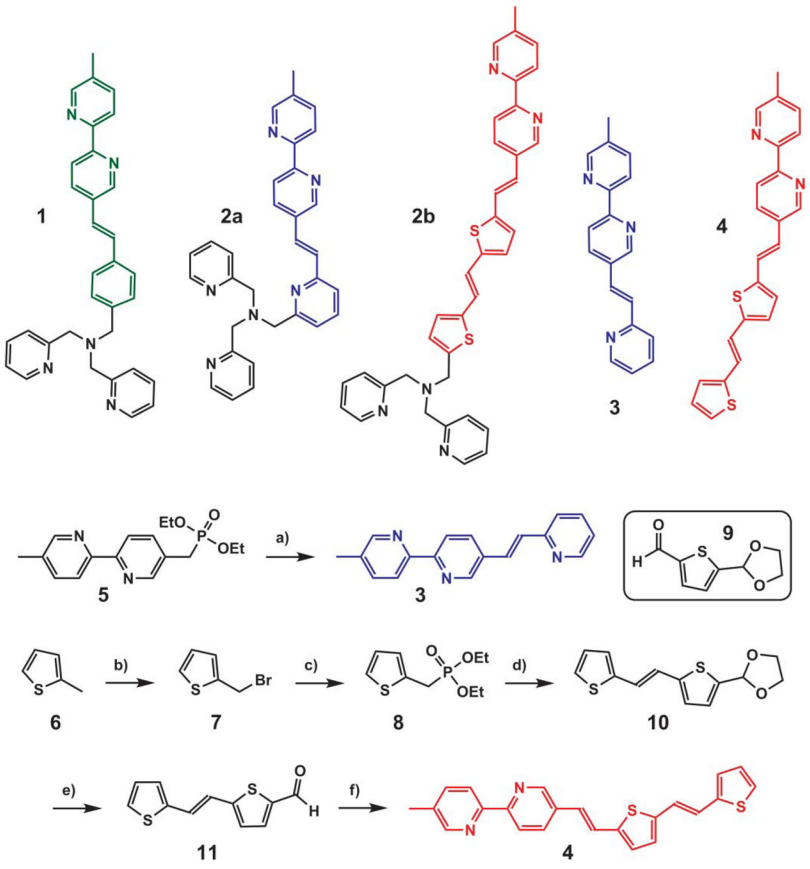

Scheme 1.

Syntheses of **3** and **4**. a) NaH, dimethoxyethane (DME), 2-pyridinecarboxaldehyde, 75%; b) NBS, benzoyl peroxide, CCl_4, 98%; c) $(EtO)_3$ P, 95%; d) **9**, NaH, DME, 25%; e) HCl–THF–H_2O; f) **5**, NaH, DME, 92% for two steps.

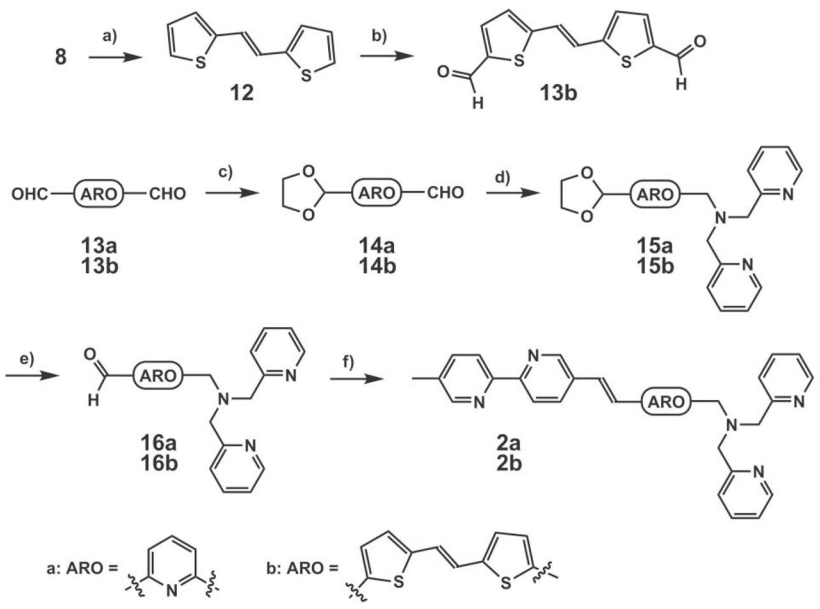

Scheme 2.

Syntheses of **2a** and **2b**. a) NaH, DME, 2-thiophene-carboxaldehyde, 88%; b) $POCl_3$, DMF, reflux, 98%; c) ethylene glycol, TsOH (catalyst), benzene, Dean–Stark, reflux, 20% for **14a**; d) di(2-picolyl)amine, $NaBH(OAc)_3$, rt, 58% for **15a**; e) HCl–THF–H_2 O, rt; f) NaH, dimethoxyethane, **5**, rt, 46% for **2a** and 12% for **2b** in two steps.

Table 1

First anodic peak potentials (E_{pa} relative to Fc/Fc^{+}), fluorescence quantum yields (φ_f) and lifetime (τ/ns) of **3**, **4**, **2a**, and **2b** and their Zn^{2+} complexes in CH_3CN.[a] λ_{ex} (**3** and **2a**) = 295 nm, λ_{ex} (**4** and **2b**) = 370 nm

ligand	E_{pa}/V	φ_f	τ/ns	φ_{Zn}	τ_1/ns	τ_2/ns
3	1.31	0.32	0.53	0.53	1.96	—
4	0.57	0.12	0.98	0.07	0.70 (69.4)	1.34 (30.6)
2a	0.65	0.01	ND[b]	0.46	1.08 (76.8)	1.98 (23.3)
2b	0.34	0.20	1.00	0.06	1.36 (93.6)	2.67 (6.39)

[a] The relative abundances of individual exponentials are in the parentheses.

[b] ND: not determined.

Table 2

Positions (λ_{abs}) and molar absorptivities (ε) of the lowest energy absorption bands of both free ligands and their Zn^{2+} complexes in CH_3 CN.[a] The Zn^{2+}-induced absorption band shifts ($\Delta\nu_{abs}/cm^{-1}$) are shown on the right along with the calculated HOMO–LUMO transition oscillator strengths (f)

ligand	λ_{abs} (L)/nm	ε(L)/$cm^{-1}M^{-1}$	λ_{abs} (ZnL)/nm	ε(ZnL)/$mol^{-1}cm^{-1}$	$\Delta\nu_{abs}/cm^{-1}$	f (HOMO–LUMO)
3	336	45 685	348	35 655	1026	1.4
4	412	54 545	430	34 805	1016	1.8
2a	340	44 911	348	30 558	676	0.2
2b	418	53 968	436	35 979	988	1.4

[a] L: free ligand; ZnL: Zn(II) complex.

Table 3

Positions (λ_{em}) of the lowest energy emission bands and Stokes shifts of both free ligands and their Zn^{2+} complexes in CH_3 CN.[a] The Zn^{2+}-induced emission band shifts ($\Delta \nu_{em}/cm^{-1}$) are shown in the rightmost column

ligand	λ_{em} (L)/nm	λ_{em} (ZnL)/nm	Stokes shift(L)/cm^{-1}	Stokes shift (ZnL)/cm^{-1}	$\Delta \nu_{em}/cm^{-1}$
3	386	420	3855	4926	2097
4	497	622	4151	7179	4044
2a	392	408	3902	4226	1,000
2b	510	605	4,316	6407	3079

[a]L: free ligand; ZnL: Zn(II) complex.